

Systematic Control of the Orientation of Organic Phosphorescent Pt complexes in Thin Films for Increased Optical Outcoupling

Jongchan Kim¹, Thilini Batagoda², Jaesang Lee¹, Daniel Sylvinson², Kan Ding⁴, Patrick Saris², Ushasree Kaipa³, Iain W. H. Oswald³, Mohammad A. Omary³, Mark E. Thompson², Stephen R. Forrest^{1,4,a}

¹ Department of Electrical Engineering and Computer Science, University of Michigan, Ann Arbor, MI, USA

² Department of Chemistry, University of Southern California, Los Angeles, CA, USA

³ Department of Chemistry, University of Northern Texas, Denson, TX, USA

⁴ Departments of Physics, and Materials Science and Engineering University of Michigan, Ann Arbor, MI, USA

^aemail: stevefor@umich.edu

Abstract

Orienting light emitting molecules relative to the substrate is an effective method to enhance the optical outcoupling of organic light emitting devices. Platinum phosphorescent complexes enable facile control of the molecular alignment due to their planar structures. Here, we control the orientation of Pt complexes during the growth of emissive layers by two different methods: modifying the molecular structure, and by using structural templating. Molecules whose structures are modified by adjusting the diketone ligand of the Pt complex, dibenzo-(f,h)quinoxaline Pt dipivaloylmethane, (dbx)Pt(dpm), show an approximately 20% increased fraction of horizontally aligned transition dipole moments compared to (dbx)Pt(dpm) doped into a 4,4'-bis(N-carbazolyl)-1,1'-biphenyl, CBP, host. Alternatively, we pre-deposited a template comprised of highly ordered 3,4,9,10-perylenetetracarboxylic dianhydride monolayers to drive the alignment of a subsequently deposited emissive layer comprising (2,3,7,8,12,13,17,18-octaethyl)-21H,23H-porphyrinplatinum(II) doped into triindolotriazine. This results in a 60% increase in horizontally aligned transition dipole moments compared to the film deposited in the absence of the template. Our findings provide a systematic route for controlling molecular alignment during layer growth, and ultimately to increase the optical outcoupling in OLEDs.

I. Introduction

To date, studies on phosphorescent emitter orientation have largely focused on Ir complexes^[1-9]. While the common Ir (III) complexes used in OLEDs have octahedral geometries, related Pt (II) complexes have planar geometries. In this context, there has been a rapid progress in developing high external quantum efficiency Pt complex emitters^[10,11] for phosphorescent organic light emitting diodes (PHOLEDs) with favorable color characteristics^[12,13], and long operational lifetimes^[14]. Highly efficient PHOLEDs using these complexes have been enabled by increasing the fraction of light outcoupled from the PHOLED by aligning the transition dipole moments (TDM) of the light emitting

This is the author manuscript accepted for publication and has undergone full peer review but has not been through the copyediting, typesetting, pagination and proofreading process, which may lead to differences between this version and the [Version of Record](#). Please cite this article as [doi: 10.1002/adma.201900921](https://doi.org/10.1002/adma.201900921).

molecules parallel to the substrate^[15–17]. Controlling the molecular alignment, therefore, can play a role in improving the efficiency of Pt complex-based PHOLEDs. The planar structure of Pt complexes has a better chance of forming π -stacking networks than bulky, 3 dimensional molecules, potentially enabling control of the molecular orientation in films via external forces such as structural templating^[18].

In this work, we control the Pt complex orientation relative to the substrate plane during the film growth using two different approaches. The first is to modify the molecular structure of heteroleptic bidentate Pt complexes to induce preferred horizontal alignment of the molecule via molecular anisotropy as illustrated in Fig. 1a. Angle dependent p-polarized photoluminescence of a film comprising (dbx)Pt(dpm) (see Fig. 1b), doped in the organic host, CBP, revealed that the dopant TDMs are preferentially oriented perpendicular to the substrate. Studies of modified complexes of (dbx)Pt(dpm) showed that the aromatic ligands control molecular orientation. The second approach achieves the preferred orientation of the emitter by pre-depositing a thin (< 2 nm) layer of a molecular template on the substrate that promotes the horizontal alignment of subsequently deposited emissive Pt complexes (Fig. 1a)^[18,19].

The relationship between TDM orientation and film morphology are investigated via a combination of angle-dependent PL and x-ray diffraction. Correlations between film crystallinity and orientation controlled via structural templating are investigated by varying the concentration of a polycrystalline host in the emissive layer, revealing that a host concentration of > 70 vol.% is required to achieve significant control over otherwise randomly distributed phosphor orientations. An increase of nearly 60% in horizontally aligned molecules is obtained using a molecular template compared with films deposited directly onto bare sapphire and fused silica substrates. We find that by varying the details of molecular and substrate structures provide a systematic route for controlling molecular alignment during layer growth, and ultimately to enhance the optical outcoupling of the emitting species, making these effective strategies for increasing OLED efficiency.

II. Results

We study a series of bidentate Pt (II) complexes with chromophoric (C^N) and ancillary (L^X) ligands, shown in Fig. 1. Density functional theory (DFT) is used to determine the TDM orientation relative to the molecular frame in these complexes. The TDM of the complex lies in the (C^N)Pt plane with an angle δ between the TDM and the Pt-N bond, which ranges between 20° and 45° for the (C^N)Pt(L^X) complexes^[20]. We chose (dbx)Pt(dpm) as the reference dopant molecule, comprising a chromophoric dibenzo-(*f,h*)-quinoxaline (dbx) aromatic ligand, and an ancillary dipivolylmethane (dpm) aliphatic ligand. The complexes are doped into CBP at 10 vol.%, and angle-dependent PL measurements of the films are analyzed to obtain the TDM orientation relative to the substrate of $\vartheta_{hor} = 0.54 \pm 0.01$, Fig. 2a. Here, ϑ_{hor} corresponds to fractional contribution of the net TDM direction lying in the horizontal plane parallel to the substrate, thus the fraction in the vertical direction is 0.46. An isotropic thin film gives $\vartheta_{hor} = 0.67$. The DFT calculation in the inset shows that $\delta = 36^\circ$. Shifting to a smaller ancillary ligand in (dbx)Pt(acac) shows similar alignment ($\vartheta_{hor} = 0.53 \pm 0.01$) to (dbx)Pt(dpm) when doped at 1 vol.% and 10 vol.% in CBP, see Fig. 2b and 2c.

Figure 3 shows the angle-dependent PL of several different (C^N)Pt(L^X) complexes doped at 10% in CBP. The film comprising (ppy)Pt(dpm) in Fig. 3a demonstrates an increased net horizontal

alignment of the TDM compared to (dbx)Pt(dpm) ($\vartheta_{hor} = 0.62 \pm 0.01$ vs. 0.54 ± 0.01). Introduction of an aromatic ancillary ligand comprising two mesityl groups attached to the acac ligand producing (dmes)Pt(dbx), increases the horizontal component even further to $\vartheta_{hor} = 0.73 \pm 0.01$. Attaching an additional Pt-dpm on the opposite side of the dbx ligand in (dbx)(Pt(dpm))₂ shown in Fig. 3c, results in a horizontal component of $\vartheta_{hor} = 0.76 \pm 0.01$.

The emission spectra of Pt-complex doped CBP films are shown in Fig. 4. Contrary to changes in the ancillary (L^X) ligand, changes in the chromophoric (C^N) ligand leads to marked shifts in the emission spectra. In contrary, promoting molecular alignment *via* substrate structural templating provides a potential route to control the orientation of the square planar Pt-complexes within a blended film without changing the molecular structure and hence its emission spectrum. Two phosphorescent Pt complexes molecules were used to explore the templating approach; one comprising a neat PtD film, and the other consisting of PtOEP doped at 10 vol.% into Tint (see Fig. 1b).

Figure 5 shows the photophysical and structural characteristics of the neat PtD, Tint, PtOEP, and PtOEP-doped Tint films on sapphire substrates. The broad PL peak at a wavelength of $\lambda_{di} = 572$ nm of neat PtD in Fig. 5a is due to dimer emission. This feature is less pronounced in PtD diluted to 1 vol.% in a PMMA host due to monomer triplet emission at $\lambda_m = 450$ -480 nm. The PtOEP-doped Tint shows dominant monomer emission at $\lambda_m = 653$ nm in Fig. 5b, with the triplet, T_1 , TDM lying within the PtOEP molecular plane (see inset), and weak dimer emission at $\lambda_{di} = 783$ nm. Monomer emission is dominant since PtOEP molecules are diluted in the host matrix. Furthermore, steric hindrance between the PtOEP ethyl groups reduces coupling between the dopants. X-ray diffraction patterns of films deposited onto a sapphire substrate in Fig. 5c exhibit intense (200), (001) and (220) diffraction peaks of PtD, PtOEP and Tint, respectively (see Supplementary Information, Fig. S1 and S2 for crystal structures and diffraction patterns of PtD and Tint).

Film morphology was also controlled via structural templating using a self-organized, 1.5nm (~5 monolayer) thick PTCDA layer^[18,21]. The PTCDA grows in the flat-lying α -phase (102) (i.e. molecular planes of PTCDA lie parallel to the substrate), thus increasing the possibility of π -stacking with the subsequently deposited molecules^[22]. For the angle-dependent PL measurement in Fig. 6a, a neat layer of NTCDA of the same thickness (1.5 nm) was deposited on the PTCDA prior to deposition of the emissive layer. The NTCDA/PTCDA bilayer transfers its structure to the subsequently deposited molecules (Fig. S4) while also blocking excitons formed in the emissive layer from quenching at PTCDA with its relatively low singlet exciton energy (1.95eV)^[23].

The PtD film deposited on the NTCDA/PTCDA template shows a decreased horizontal orientation ($\vartheta_{hor} = 0.33 \pm 0.01$) of the PtD dimer TDM compared to deposition on a bare fused silica substrate with $\vartheta_{hor} = 0.91 \pm 0.01$ (see Fig. 6a). To determine the relationship between TDM orientation and film morphology, x-ray pole figures of the (200) and (020) planes are provided in Fig. 6b and 6c. The configuration of each plane within the PtD crystal is shown in Fig. 6d. The film deposited directly on the sapphire substrate in Fig. 6b shows the (200) diffraction peak ($2\vartheta=8.2$ -8.5°) at a radial angle of $\psi = 0^\circ$, suggesting that (200) plane lies parallel to the substrate. The (200) plane lies perpendicular to the PtD molecular plane, hence the (200) diffraction peak at $\psi = 0^\circ$ indicates the molecular plane is vertically aligned to the substrate. The (020) plane ($2\vartheta = 26.6^\circ$) parallel to the molecular plane shows a diffraction peak at $\psi = 0^\circ$ for the film on the template layer, indicating that the PtD molecules lie

with their molecular planes parallel to the templating molecules. The x-ray diffraction patterns of the 30 nm thick film of PtD deposited on sapphire, ITO and PTCDA are shown in Fig. S5.

The volume fraction of crystal domains within a CzSi film blended with PtD was measured as a function of doping concentration, with results shown in Fig. 7a. Vacuum deposited films of neat CzSi result in isotropic orientation (Fig. S6). A decreasing intensity and increasing full-width at half-maximum of the XRD peak^[24] with decreasing PtD concentration indicates decreased film crystallinity and PtD domain size, as shown in Table 1. The TDM alignment measured by angle-dependent PL for each PtD:CzSi blend is shown in Fig. 7b. The alignment is random ($\vartheta_{hor} \sim 66\%$) at concentrations < 10 vol.%, while for the neat PtD film, an ordered morphology with $\vartheta_{hor} > 90\%$ is achieved. The TDM orientation was also measured for PtD:CzSi blends with a range of concentrations deposited on the NTCDA/PTCDA template, showing the controlled morphology of the film at PtD concentration of > 70 vol.%.

The orientation of the blended film comprising PtOEP doped in Tint at 10 vol.% deposited on the template and on a bare sapphire substrate are compared by x-ray diffraction in Fig. 8a. A monolayer of PTCDA is used as a template layer for x-ray diffraction. The neat Tint film deposited on the template compared to the bare substrate shows a peak shift from $2\vartheta=27.0^\circ$ to $2\vartheta=27.5^\circ$, corresponding to a morphological change from $(\bar{2}20)$ to (120) diffraction plane. This peak shift of Tint molecules is also observed in the PtOEP:Tint blends. In the blended films, PtOEP peaks also shift when deposited on the template, from $2\vartheta=25.7^\circ$ to $2\vartheta=20.5^\circ$, corresponding to a change from (212) to $(1\bar{1}\bar{1})$ plane. The crystal structures and diffraction planes of PtOEP and Tint are shown in Fig. 8b and c. We also measured the TDM orientation of the blended film deposited on the NTCDA/PTCDA template showing an increased ϑ_{hor} compared to a bare substrate, from 0.22 ± 0.02 to 0.80 ± 0.01 as shown in Fig. 8d.

III. Discussion

The orientation of heteroleptic bidentate Pt complexes demonstrate the relative interactions of the two ligands with the organic surface. Specifically, if the interaction of both ligands with the surface is relatively weak, the molecular orientation is random. If the interaction of both ligands is similarly strong, a horizontal orientation relative to the substrate is promoted. However, if one ligand has a stronger interaction with the organic surface than the other, the molecule aligns vertically. Another possible way for the dopant molecule to self-organize is by aggregation with adjacent molecules forming polycrystalline islands within the film^[25].

In Fig. 2a, the TDM of $(dbx)Pt(dpm)$ shows a disproportionate vertical orientation. Since $\delta = 36.1^\circ$ is close to the c_2 axis, the vertically aligned TDM shows that one ligand of the $(dbx)Pt(dpm)$ has a markedly stronger interaction via edge-to-surface π - π interactions with the organic surface. To confirm that the vertical alignment is not due to aggregation, $(dbx)Pt(acac)$ was doped at 10 and 1 vol.% into the host matrix in Fig. 2b and 2c. The ancillary dpm ligand was replaced by an acac ligand to promote aggregation, which is evident from the red-shifted spectrum of the 10 vol.% film in Fig. 4. As a result, $(dbx)Pt(acac)$ doped at 1 vol.% showed similar alignment ($\vartheta_{hor} = 0.53 \pm 0.01$) to the 10 vol.% doped $(dbx)Pt(acac)$ and $(dbx)Pt(dpm)$ with no spectral red-shift. The similar orientation of $(dbx)Pt(acac)$ with $(dbx)Pt(dpm)$, regardless of the doping concentration, shows that the vertical orientation of the Pt complexes is not due to the dopant aggregation.

It is known that the intermolecular interaction strength is directly proportional to the size of the aromatic system^[26]. Therefore, the smaller aromatic surface of ppy compared to dbx leads to a weaker interaction of (ppy)Pt(dpm) with the organic surface than the dbx based materials, and hence a reduced vertical molecular orientation relative to (dbx)Pt(dpm). To investigate whether the fraction of aromatic surface area in the ligand is tied to the molecular alignment, (dbx)Pt(dmes) with C[^]N and L[^]X ligands having substantial aromatic character. The horizontal component increased to $\vartheta_{hor} = 0.73 \pm 0.01$, leading to a net preferred horizontal alignment. The emission spectrum was unchanged since the chromophoric ligand also remained unchanged (Fig. 4). Adding a second Pt(dpm) to the dbx ligand producing (dbx)(Pt(dpm))₂ results in a further increase in ϑ_{hor} to 0.76 ± 0.01 , Fig. 3c, relative to (dbx)Pt(dpm). This is contrary to the hypothesis that the lower aromatic fraction of (dbx)(Pt(dpm))₂ promotes perpendicular alignment. Unlike the (C[^]N)Pt(L[^]X) complexes, the TDM of (dbx)(Pt(dpm))₂ lies at $\delta = -11^\circ$ relative to the Pt-N and Pt-C bonds (see inset, Fig. 3c). If (dbx)(Pt(dpm))₂ is aligned perpendicular to the substrate, ϑ_{hor} is close to unity. The spectrum of (dbx)(Pt(dpm))₂ red shifts due to the extended π -conjugation of the larger ligand^[27,28].

The work of Hunter and Sanders^[29,30] suggests that the (dbx)Pt(dpm) molecule achieves vertical orientation via a balance between π - σ attraction (the attraction of the negatively charged π -electrons and a positively charged σ -framework), and π -electron repulsion. The edge-on geometry requires a strong π - σ attraction, whereas π - π repulsion and quadrupole attraction dominates in a cofacial, π -stacked geometry^[31,32]. The dbx ligand shows a high net positive σ -framework due to the electron deficient π -system caused by two electron-withdrawing N atoms^[32], leading to its edge-on geometry. We calculated the electrostatic potential surface of (dbx)Pt(dpm) in Fig. S7 to compare the relative π - σ attraction of the two ligands. The average potential of the dbx ligand σ -framework shows 12.3 kcal/mol, with a peak potential of 17.9 kcal/mol near the N atoms. On the other hand, the dpm ligand shows an average 3.5 kcal/mol.

Pt complex molecules have planar structures, leading to strong π - π interactions with the surrounding environment, such as the host molecules. Thus, the orientation of the Pt complex dopants is influenced by the host matrix. According to Huh et al.^[33], there is a lower fraction of horizontally aligned TDMs for Pt dopants in CBP compared to the other hosts. Therefore, changing the host molecule from CBP may increase the fraction horizontal alignment of Pt dopant molecules.

Density functional theory was used to investigate the relationship between the TDM of the PtD dimer and the molecular orientation in a neat crystalline PtD film (see Fig. 6). Calculations indicate that the TDM of the dimer lies perpendicular to the PtD monomer planes. The crystal structure of PtD features two unique emissive dimer configurations: one with a Pt-Pt separation of 3.35 Å and the other with 3.41 Å, henceforth referred to as 3.35-dimer and 3.41-dimer, respectively. The energy of the 3.35-dimer triplet (T_1) is 2.25 eV, compared with 2.27 eV for the 3.41-dimer (details found in Fig. S8). Also, the oscillator strength computed for T_1 of the former is almost twice that of the latter, indicating that emission in neat crystalline PtD films is likely to originate predominantly from the 3.35-dimer. The red arrow in Fig. 5a, inset, indicates that the 3.35-dimer TDM subtends a polar angle of 10° with the z-axis which lies along the Pt-Pt axis, and at an azimuthal angle of 99° with the x-axis that passes through the Pt-N(pyrazole-ring) bond of one of the monomers. The results from the DFT calculation and XRD data show that the TDM orientation is indeed controlled via templating.

In Fig. 7a, the PtD (200) diffraction peak shifts toward an increased lattice constant with the reduced PtD domain size. The increased density of grain boundaries for smaller grains results in an increased lattice constant compared to bulk single crystals as a result of lattice strain relaxation^[34]. The relaxed lattice also results in the hypsochromic shift of the dimer emission (Fig. S9), with results summarized in Table 1.

Time-resolved photoluminescence of the films of PtD doped into CzSi at various doping concentrations was measured with results in Fig. S10. The data show a broad photoluminescence peak at $\lambda = 572$ nm that originates from the dimeric species. At 1 vol.% PtD, a monomer peak appears at $\lambda = 450$ nm (Fig. S9), showing biexponential decay with distinct exciton decay lifetimes ($\tau_{dimer} = 0.88 \pm 0.12$ vs. $\tau_{monomer} = 0.10 \pm 0.01$), as shown in Fig. S10. This feature shows that monomer and dimer excitons coexist in 1 vol.% film, which corresponds to the spectrum in Fig. S9. However, single exponential decay is observed at higher doping concentrations with exciton lifetimes similar to the dimer exciton at 1 vol.%. Since only a broad photoluminescence peak at $\lambda = 550$ nm is observed at these higher concentrations, we conclude that the broad photoluminescence originates from dimer emission.

The TDM orientation was measured for PtD:CzSi blends with a range of concentrations deposited on the NTCDA/PTCDA template in Fig. 7b. The XRD results in Fig. 7a show that PtD molecules form highly crystalline films due to their discotic molecular structure that enables efficient π -stacking. In the PtD:CzSi blend, however, the CzSi molecules interrupt the π -stacking of the PtD molecules at CzSi concentrations >30 vol.%, and hence the orientation of the template is not transferred to the PtD molecules. In contrast, for CzSi concentrations < 30 vol.%, the disruption of the stacks is limited, enabling the efficient transfer of the template orientation to PtD. Therefore, a concentration of polycrystalline discotic host molecule of > 70 vol.% is required to control the morphology of the blended film.

Figure 8a shows the controlled morphology of PtOEP doped in Tint deposited with the PTCDA template by x-ray diffraction. The x-ray diffraction peaks of Tint ($\bar{2}20$) and PtOEP (212) planes in the film are shifted compared to the bulk (Tint ($\bar{2}20$), $2\theta = 27.2^\circ$; PtOEP (212), $2\theta = 26.0^\circ$) due to the lattice relaxation at grain boundaries. The blended film deposited on the bare substrate shows the edge-on diffraction for both Tint and PtOEP molecules (Fig. 8b and 8c, green)^[35]. This geometry is caused by aggregation with adjacent molecules forming polycrystalline islands in the film, as Loi et al. showed with the α -sexithiophene^[27]. A neat Tint film on a PTCDA template shows its largest diffraction feature for the (120) plane, which is due to Tint crystallites (Fig. 8b, red) lying parallel to the substrate. The reorientation is due to matching to the α -phase PTCDA template ($2\theta = 27.5^\circ$) with a strain of $(a_{film} - a_{temp}) / a_{temp} = 0.7\%$, where a_{film} and a_{temp} are lattice constants of the Tint and PTCDA layers, respectively. Note that a peak appears at $2\theta = 27.5^\circ$ which corresponds to the α -phase PTCDA. Similarly, the PtOEP diffraction peak shifts to $2\theta = 20.5^\circ$, consistent with the (1 $\bar{1}\bar{1}$) plane being parallel to the substrate (Fig. 8c, red). This morphological control of the PTCDA template was also demonstrated via doped film deposited on the NTCDA/PTCDA template and bare substrate, showing an increased ϑ_{hor} from 0.22 ± 0.02 to 0.80 ± 0.01 (Fig. 8d), consistent with the x-ray diffraction data.

Although PTCDA plays a central role in initiating structural templating, it has a low exciton energy, and therefore tends to quench excitons formed within the emissive layer. Identifying a molecule that

has optimal energetics for an OLED while showing similar morphological characteristics as PTCDA remains a challenge.

IV. Conclusions

We demonstrated that the interaction between the aromatic regions of the ligands and the organic surface drives the orientation of dihedral phosphor Pt complexes during the vacuum deposition. Accordingly, the molecular structure of the vertically aligning reference Pt complex, (dbx)Pt(dpm), was modified to increase the fraction of horizontally aligned TDM in the blended film. In one example, we introduced two mesityl groups to the ancillary ligand to increase the attraction of the molecule to the organic surface. In a second approach, the TDM of a binuclear Pt complex, (dbx)(Pt(dpm))₂, was shown to align parallel to the substrate due to the attraction of its aromatic region. Both methods showed an approximately 20% increased fraction of horizontally aligned TDMs compared to the reference Pt complex.

We also found that seeding the growth habit of the molecules in the blended emissive layer via an ordered NTCDA/PTCDA template results in a preferred horizontal alignment of the Pt phosphor emitter molecules. Polycrystalline emissive layers comprising single molecule or mixed host-dopant molecules were both shown to conform to the template orientation. The net horizontal fraction of the dopant transition dipole moment in the mixed host-dopant layer deposited on the template increased by approximately 60% compared to the film deposited directly onto bare sapphire and fused silica substrates. Our findings demonstrate an efficient molecular design strategy and a method to control the optical outcoupling efficiencies of the organic light emitting devices comprising Pt complex phosphors.

V. Methods

Nomenclatures. The abbreviations used for molecules are as follows. Acetylacetonate (acac), 4,4'-bis(N-carbazolyl)-1,1'-biphenyl (CBP), 9-(4-tert-butylphenyl)-3,6-bis(triphenylsilyl)-9H-carbazole (CzSi), dibenzo-(f,h)quinoxaline (dbx), 1,3-dimesitylpropane-1,3-dione (dmes), dipivaloylmethane (dpm), 1,4,5,8-naphthalenetetracarboxylic dianhydride (NTCDA), poly-methylmethacrylate (PMMA), 2-phenylpyridinate (ppy), 3,4,9,10-perylenetetracarboxylic dianhydride (PTCDA), (3-(trifluoromethyl))(5-(pyridyl)-pyrazolate 5-pyridyl-tetrazolate) Pt(II) (PtD), (2,3,7,8,12,13,17,18-octaethyl)-21H,23H-porphyrinplatinum(II) (PtOEP), triindolotriazine (Tint).

Sample preparation. Thin films were deposited at 1.0 Å/s on 0.2 mm thick fused silica glass by vacuum thermal evaporation in a chamber with a base pressure of 1×10^{-7} torr. The deposition rate and film thicknesses were controlled using a quartz crystal thickness monitor. Following deposition, devices were encapsulated using an epoxy seal around the edge of a cover glass in a N₂ environment. The samples for angle-dependent optical characterization consist of 1.5 nm PTCDA / 1.5 nm NTCDA/ 30 nm emissive layer. PTCDA, NTCDA, PtOEP, and CBP were purchased from Luminescence Technology, Corp.

Optical measurements. Samples were excited with a He-Cd laser at a wavelength of 325nm. Alignment of the transition dipole moment (TDM) was inferred from the angle-resolved photoluminescence of the phosphor-doped films^[36,37]. The emission from horizontally aligned TDMs is decomposed into transverse electric (TE_{hor}) and magnetic (TM_{hor}) modes, whereas the vertically aligned TDM emits into the TM_{ver} mode. The ratio of horizontal-to-vertical transition dipole moments (ϑ_{hor}) is:

$$\theta_{hor} = \frac{TE_{hor} + TM_{hor}}{TE_{hor} + TM_{hor} + TM_{ver}},$$

leading to $\vartheta_{hor} = 0.67$ for random alignment ($TE_{hor} = TM_{hor} = TM_{ver}$), and $\vartheta_{hor} = 1.0$ for TDMs oriented parallel to the substrate.

The ϑ_{hor} was obtained from the intensity ratio of TM_{hor} to TM_{ver} modes by removing TE_{hor} using a polarization filter. This is compared to the simulated values calculated based on the dyadic Green's function in a birefringent medium^[38]. A least-squares algorithm was used to fit the measured photoluminescence data to the simulation. The 0.2 mm thick fused silica substrate was placed perpendicular to the plane of detection and the emission was outcoupled from the substrate using a 2 cm radius, half-cylindrical lens. A motorized stage was used to position the detector. The refractive indices and extinction coefficients of materials were measured using variable-angle spectroscopic ellipsometry.

X-ray diffraction measurements. X-ray measurements for thin film samples were performed in the Bragg-Brentano geometry using the Cu-K α radiation source operated at 40kV and 44mA in a Rigaku Ultima IV X-Ray Diffractometer.

Single crystal structure determination. The plates of PtD, Tint and (dbx)Pt(dpm) were grown by 3-zone thermal gradient vacuum sublimation. The zone temperatures for PtD and Tint were 240 / 210 / 180 °C and 200 / 165 / 135 °C, respectively. For PtD and Tint crystals of dimensions of 0.04 × 0.01 × 0.01 mm and 0.01 × 0.01 × 0.01 mm were mounted on a Rigaku AFC10K Saturn 944+ CCD-based X-ray diffractometer equipped with a low temperature device and Micromax-007HF Cu-target micro-focus rotating anode ($\lambda = 1.54187 \text{ \AA}$) operated at 1.2 kW (40 kV, 30 mA). The X-ray intensities were measured at 85 K with the detector placed at a distance 42.00 mm from the crystal. Rigaku d*trek images were exported to CrysAlisPro for processing and corrected for absorption. A transparent, prism-like 0.11 mm x 0.18 mm x 0.35 mm crystal of (dbx)Pt(dpm) was used for the X-ray crystallographic analysis. The X-ray intensity data are obtained using a Bruker APEX DUO system equipped with a fine-focus tube (MoK α , $\lambda = 0.71073 \text{ \AA}$) and a TRIUMPH curved-crystal monochromator. The frames were integrated with the SAINT V8.37A (Bruker AXS, 2013) algorithm. Data were corrected for absorption using the multi-scan method (SADABS). The structures for the three compounds were solved and refined with the Bruker SHELXTL (version 2016/6) software package. Additional details are given in CIF files.

DFT calculations of TDM and molecular orbitals. The ground (S_0) and triplet state (T_1) geometries of PtD and PtOEP were optimized at the B3LYP/LACV3P** level using the Jaguar (v. 9.4 release 15) program within the Material Science suite developed by Schrödinger, LLC^[39]. Time-dependent density functional theory (TD-DFT) with the zero order regular approximation (ZORA) approach^[40] as

implemented in Jaguar to compute the TDMs for phosphorescent ($T_1 \rightarrow S_0$) emission,. The ZORA Hamiltonian incorporates spin-orbit coupling (SOC) effects that are associated with triplet ($T_1 \rightarrow S_0$) emission. The SOC-TD-DFT calculations were performed on the T_1 optimized structures using the B3LYP functional and a mixed basis set in which the DYALL-2ZCVP-ZORA-J-Pt-Gen set was used for the Pt ,while the 6-31G** set was used for the remainder of the atoms.

To simulate the T_1 state relaxation of the PtD excimers/dimers (3.41-dimer and 3.35-dimer) within the crystalline matrix, geometry optimization was performed on each dimer constrained by a molecular shell consisting of all its immediate neighbors (based on the crystal structure packing data) modeled as a rigid classical force field. This was done using a 2-layer hybrid QM/MM with a n -layered integrated molecular orbital and molecular mechanics (NIOM) scheme in which the central dimer was treated at the B3LYP/LanL2Dz level while the UFF molecular mechanics force field was used to model the surrounding molecular shell which was kept frozen during the optimization. All NIOM calculations were performed using the Gaussian 09 program^[41]. Subsequently, SOC-TDDFT calculations were performed on the T_1 (NIOM:B3LYP/LanL2Dz:UFF) optimized structure of both dimers to obtain the TDVs associated with dimeric/excimeric emission. The surrounding molecular shell was ignored for the SOC-TDDFT calculations.

Synthesis. Information for the molecular synthesis are included in the Supplementary Information, Fig. S11.

Supporting Information

Details are provided for synthetic, characterization and density functional theory calculations for the platinum complexes, crystal structure information for PtD, Tint and (dbx)Pt(dpm), variable angle spectroscopic ellipsometry data for templated a NTCDa and CzSi films, Bragg-Brentano x-ray diffraction patterns of PtD thin film on different substrates and emission spectra of CzSi:PtD at a range of doping concentrations.

Acknowledgements

The work was supported by the Office of Energy Efficiency and Renewable Energy (EERE), U.S. Department of Energy, under Award Number DE-EE0007626 and Universal Display Corporation. We thank Dr. Zhongrui Li and Dr. Kai Sun for the helpful comments and suggestions. We thank Dr. Jeff Kampf and Dr. Ralf Haiges for help with the crystallographic studies of Tint, PtD and (dpm)Pt(dbx). M.A.O. gratefully acknowledges support by the Welch Foundation (Grant B-1542) and the U.S. National Science Foundation (Grant CHE-1413641).

References

- [1] M. Flämmich, J. Frischeisen, D. S. Setz, D. Michaelis, B. C. Krummacher, T. D. Schmidt, N. Danz, W. Brütting, *Org. Electron.* **2011**, *12*, 1663.
- [2] K.-H. Kim, S. Lee, C.-K. Moon, S.-Y. Kim, Y.-S. Park, J.-H. Lee, J. Woo Lee, J. Huh, Y. You, J.-J. Kim, *Nat. Commun.* **2014**, *5*, 4769.
- [3] P. Liehm, C. Murawski, M. Furno, B. Lüssem, K. Leo, M. C. Gather, *Appl. Phys. Lett.* **2012**, *101*, 253304.
- [4] H. Shin, J.-H. Lee, C.-K. Moon, J.-S. Huh, B. Sim, J.-J. Kim, *Adv. Mater.* **2016**, 4920.
- [5] A. Graf, P. Liehm, C. Murawski, S. Hofmann, K. Leo, M. C. Gather, *J Mater Chem C* **2014**, *2*, 10298.
- [6] M. J. Jurow, C. Mayr, T. D. Schmidt, T. Lampe, P. I. Djurovich, W. Brütting, M. E. Thompson, *Nat. Mater.* **2016**, *15*, 85.
- [7] C.-K. Moon, K.-H. Kim, J.-J. Kim, *Nat. Commun.* **2017**, *8*, 791.
- [8] T. Lee, B. Caron, M. Stroet, D. M. Huang, P. L. Burn, A. E. Mark, *Nano Lett.* **2017**, *17*, 6464.
- [9] C. Mayr, W. Brütting, *Chem. Mater.* **2015**, *27*, 2759.
- [10] K.-H. Kim, J.-L. Liao, S. W. Lee, B. Sim, C.-K. Moon, G.-H. Lee, H. J. Kim, Y. Chi, J.-J. Kim, *Adv. Mater.* **2016**, *28*, 2526.
- [11] K. T. Ly, R.-W. Chen-Cheng, H.-W. Lin, Y.-J. Shiau, S.-H. Liu, P.-T. Chou, C.-S. Tsao, Y.-C. Huang, Y. Chi, *Nat. Photonics* **2017**, *11*, 63.
- [12] T. Fleetham, Z. Wang, J. Li, *Org. Electron.* **2012**, *13*, 1430.
- [13] G. E. Norby, C.-D. Park, B. O'Brien, G. Li, L. Huang, J. Li, *Org. Electron.* **2016**, *37*, 163.
- [14] T. B. Fleetham, L. Huang, K. Klimes, J. Brooks, J. Li, *Chem. Mater.* **2016**, *28*, 3276.
- [15] V. Bulović, V. B. Khalfin, G. Gu, P. E. Burrows, D. Z. Garbuzov, S. R. Forrest, *Phys. Rev. B* **1998**, *58*, 3730.
- [16] L. H. Smith, J. a. E. Wasey, I. D. W. Samuel, W. L. Barnes, *Adv. Funct. Mater.* **2005**, *15*, 1839.

- [17] S. Nowy, B. C. Krummacher, J. Frischeisen, N. A. Reinke, W. Brütting, *J. Appl. Phys.* **2008**, *104*, 123109.
- [18] B. E. Lassiter, R. R. Lunt, C. K. Renshaw, S. R. Forrest, *Opt. Express* **2010**, *18*, A444.
- [19] K. S. Yook, B. D. Chin, J. Y. Lee, B. E. Lassiter, S. R. Forrest, *Appl. Phys. Lett.* **2011**, *99*, 043308.
- [20] Y. Chi, P.-T. Chou, *Chem. Soc. Rev.* **2010**, *39*, 638.
- [21] K. Xiao, W. Deng, J. K. Keum, M. Yoon, I. V. Vlassiouk, K. W. Clark, A.-P. Li, I. I. Kravchenko, G. Gu, E. A. Payzant, B. G. Sumpter, S. C. Smith, J. F. Browning, D. B. Geohegan, *J. Am. Chem. Soc.* **2013**, *135*, 3680.
- [22] S. R. Forrest, *Chem. Rev.* **1997**, *97*, 1793.
- [23] V. R. Gangilenka, L. V. Titova, L. M. Smith, H. P. Wagner, L. A. A. DeSilva, L. Gisslén, R. Scholz, *Phys. Rev. B* **2010**, *81*, 155208.
- [24] A. L. Patterson, *Phys. Rev.* **1939**, *56*, 978.
- [25] M. A. Loi, E. da Como, F. Dinelli, M. Murgia, R. Zamboni, F. Biscarini, M. Muccini, *Nat. Mater.* **2005**, *4*, 81.
- [26] E. R. Vorpagel, J. G. Lavin, *Carbon* **1992**, *30*, 1033.
- [27] K. Hanson, L. Roskop, P. I. Djurovich, F. Zahariev, M. S. Gordon, M. E. Thompson, *J. Am. Chem. Soc.* **2010**, *132*, 16247.
- [28] T. Sajoto, P. I. Djurovich, A. Tamayo, M. Yousufuddin, R. Bau, M. E. Thompson, R. J. Holmes, S. R. Forrest, *Inorg. Chem.* **2005**, *44*, 7992.
- [29] C. A. Hunter, J. K. M. Sanders, *J. Am. Chem. Soc.* **1990**, *112*, 5525.
- [30] C. A. Hunter, K. R. Lawson, J. Perkins, C. J. Urch, *J. Chem. Soc. Perkin Trans. 2* **2001**, 651.
- [31] M. O. Sinnokrot, C. D. Sherrill, *J. Am. Chem. Soc.* **2004**, *126*, 7690.
- [32] C. Janiak, *J. Chem. Soc. Dalton Trans.* **2000**, 3885.
- [33] J.-S. Huh, K.-H. Kim, C.-K. Moon, J.-J. Kim, *Org. Electron.* **2017**, *45*, 279.
- [34] E. J. Mittemeijer, P. Scardi, *Diffraction Analysis of the Microstructure of Materials*, **2010**.
- [35] L. R. Milgrom, R. N. Sheppard, A. M. Z. Slawin, D. J. Williams, *Polyhedron* **1988**, *7*, 57.

- [36] J. Frischeisen, D. Yokoyama, C. Adachi, W. Brütting, *Appl. Phys. Lett.* **2010**, *96*, 073302.
- [37] C.-K. Moon, S.-Y. Kim, J.-H. Lee, J.-J. Kim, *Opt. Express* **2015**, *23*, A279.
- [38] K. Celebi, T. D. Heidel, M. A. Baldo, *Opt. Express* **2007**, *15*, 1762.
- [39] A. D. Bochevarov, E. Harder, T. F. Hughes, J. R. Greenwood, D. A. Braden, D. M. Philipp, D. Rinaldo, M. D. Halls, J. Zhang, R. A. Friesner, *Int. J. Quantum Chem.* **2013**, *113*, 2110.
- [40] E. van Lenthe, E. J. Baerends, J. G. Snijders, *J. Chem. Phys.* **1993**, *99*, 4597.
- [41] M. J. Frisch, G. W. Trucks, J. R. Cheeseman, G. Scalmani, M. Caricato, H. P. Hratchian, X. Li, V. Barone, J. Bloino, G. Zheng, T. Vreven, J. A. Montgomery, G. A. Petersson, G. E. Scuseria, H. B. Schlegel, H. Nakatsuji, A. F. Izmaylov, R. L. Martin, J. L. Sonnenberg, J. E. Peralta, J. J. Heyd, E. Brothers, F. Ogliaro, M. Bearpark, M. A. Robb, B. Mennucci, K. N. Kudin, V. N. Staroverov, R. Kobayashi, J. Normand, A. Rendell, R. Gomperts, V. G. Zakrzewski, M. Hada, M. Ehara, K. Toyota, R. Fukuda, J. Hasegawa, M. Ishida, T. Nakajima, Y. Honda, O. Kitao, H. Nakai, *Gaussian 09*, n.d.

Table I: Thin film morphology of CzSi films doped with PtD

Doping Concentration [vol.%]	Peak 2ϑ [°] ^(a)	FWHM [°] ^(b)	d-spacing ^(c) [Å]	Crystallite Size ^(d) [nm]	θ_{hor}	
					Non-Templated	Templated
100	8.35	0.40 ± 0.01	10.6	20.8 ± 0.5	0.91 ± 0.01	0.33 ± 0.01
90	8.30	0.55 ± 0.01	10.6	15.1 ± 0.3	0.88 ± 0.03	0.66 ± 0.01
70	8.23	1.04 ± 0.02	10.7	8.0 ± 0.2	0.86 ± 0.02	0.82 ± 0.02
50	8.12	1.28 ± 0.01	10.9	6.5 ± 0.1	0.79 ± 0.01	0.82 ± 0.02

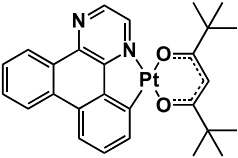
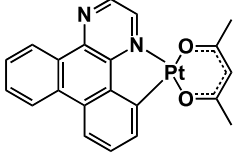
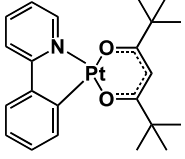
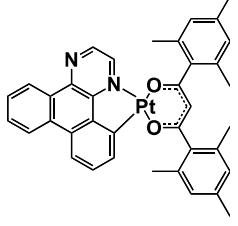
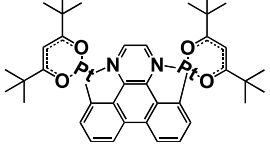
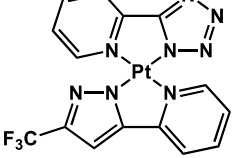
(a) Random error = $\pm 0.03^\circ$

(b) Calculation based on Gaussian Fitting model

(c) Random error = $\pm 0.1 \text{ \AA}$

(d) Calculated utilizing Debye-Scherrer equation, $t = K\lambda/\beta\cos\vartheta$, where K is a crystallite shape dependent constant (0.94), $\lambda = 1.54\text{\AA}$ is the wavelength of Cu- α x-ray source, β is the full width at half maximum of the peak, and ϑ is the Bragg angle.

Table II: Structural and emission data of reference Pt complexes

	Structure	Monomer Peak [nm]	Dimer Peak [nm]
(dbx)Pt(dpm)		563.82	-
(dbx)Pt(acac)		551.12	715.85
(ppy)Pt(dpm)		494.37 (First Peak)	-
(dbx)Pt(dmes)		559.67	-
(dbx)(Pt(dpm)) ₂		638.82	-
PtD		446.43 (First Peak)	572

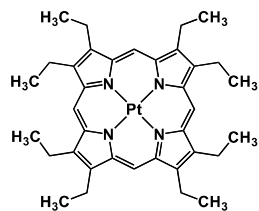


Figure captions

Figure 1: Controlling molecular orientation in light emitting layers. **a.** Amorphous growth leads to random alignment of molecules relative to the substrate (left). Molecular anisotropy can lead to preferable alignment of light emitting species (middle). Growth of an ultrathin templating layer forces the subsequently deposited molecules to lie flat on the substrate (right). **b.** Molecular structural formulae of the Pt complexes and small molecules used for the experiments are shown.

Figure 2: Orientation analysis of (dbx)Pt(dpm). Angle dependent *p*-polarized photoluminescence measurements for **a.** (dbx)Pt(dpm) doped at 10 vol.% and (dbx)Pt(acac) doped at **b.** 1vol.%, and **c.** 10 vol.% into a CBP host. Insets show the TDM orientations in the molecules.

Figure 3 Orientation analysis of Pt complex dopants. Angle dependent *p*-polarized photoluminescence measurement for **a.** (ppy)Pt(dpm), **b.** (dbx)Pt(dmes), and **c.** (dbx)(Pt(dpm))₂ doped into CBP at 10 vol.%. Insets show the TDM orientations in the molecules.

Figure 4 Photoluminescence spectra of films of Pt complexes doped into CBP. Measured photoluminescence of films of (dbx)Pt(dpm), (dbx)Pt(acac), (ppy)Pt(dpm), (dbx)Pt(dmes) and (dbx)(Pt(dpm))₂ doped into CBP at 10 vol.%. The (dbx)Pt(acac) was also doped into CBP at 1 vol.%.

Figure 5: Photophysical and structural characteristics of neat films of PtD and PtOEP doped Tint. **a.** Photoluminescence spectra of films of neat PtD, and 1 vol.% PtD doped in PMMA. The arrow in the inset illustrates the dimer transition dipole moment vector formed between two PtD molecules as determined via time dependent density functional theory (TD-DFT). The *z*-axis is between the Pt center of the dopant molecules, whereas the PtD molecular plane lies in the *x*-*y* plane. **b.** Photoluminescence spectra of PtOEP doped Tint at 10 vol.%. The arrow in the inset illustrates the transition dipole moment vector within the PtOEP molecule. **c.** XRD diffraction patterns of neat PtOEP, PtD and Tint films. The data are offset for clarity.

Figure 6: Control of the PtD transition dipole moment via templating. **a.** Angle-dependent *p*-polarized photoluminescence of a neat PtD film grown on sapphire substrate and on a pre-deposited template layer. **b.** X-ray pole figure of the (200) plane ($2\theta = 8.4^\circ$) for a neat PtD film on sapphire. **c.** X-ray pole figure of the (020) plane ($2\theta = 26.6^\circ$) for a neat PtD film on a PTCD A template layer. **d.** PtD crystal structure showing the (200) (green) and (020) (red) planes.

Figure 7: Relation between crystallinity and structural templating. **a.** XRD patterns of PtD doped CzSi films as a function of PtD concentration. Background counts of the 50 vol.% PtD:CzSi film removed for clarity. **b.** Measured ϑ_{hor} for the dimer emission transition dipole moment of PtD versus

concentration in CzSi. The blue and red curves show ϑ_{hor} of films deposited on a bare substrate and on a pre-deposited PTCD A template, respectively.

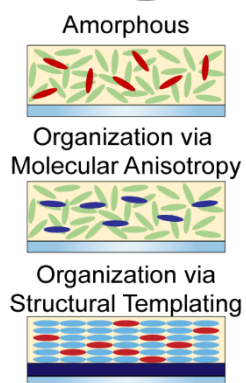
Figure 8: Control of the PtOEP:Tint transition dipole moment via templating. **a.** XRD patterns of the films with neat and blended Tint with PtOEP deposited on the template layer and on a bare sapphire substrate. Data are offset for clarity. **b.** Tint crystal structure and diffraction planes from single crystal x-ray diffraction measurements. The diffraction peaks at $2\vartheta = 27.0^\circ$ and 27.3° correspond to the $(\bar{2}20)$ plane (green), (120) plane (red), respectively. **c.** PtOEP crystal structure and diffraction planes from Cambridge Crystallographic Data library (CCDC-1167542). The diffraction peaks at $2\vartheta = 25.9^\circ$ and 20.5° correspond to (212) (green), $(\bar{1}\bar{1}\bar{1})$ (red) planes, respectively. **d.** Angle dependent p-polarized photoluminescence of PtOEP:Tint films.

Author Manuscript

Table of Contents Text

The orientation of Pt complexes is controlled by modifying the molecular structure and by structural templating. Molecules with modified structures show an approximately 20% increased fraction of horizontally aligned transition dipole moments (TDMs) when doped into a host matrix. Alternatively, a highly ordered molecular template drives the alignment of a subsequently deposited polycrystalline emissive layer, showing a 60% increase in horizontally aligned TDMs compared to the film deposited without the template.

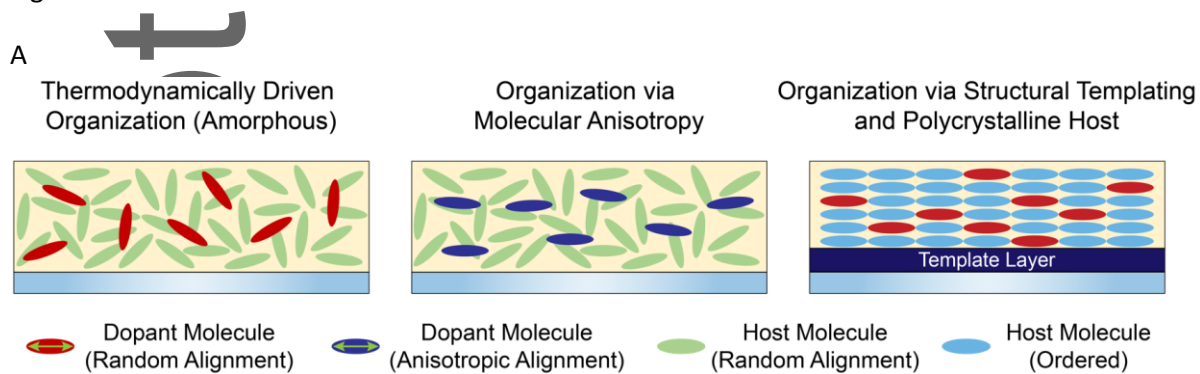
Table of Contents Figure



Author Manuscript

Figure

Figure 1



B

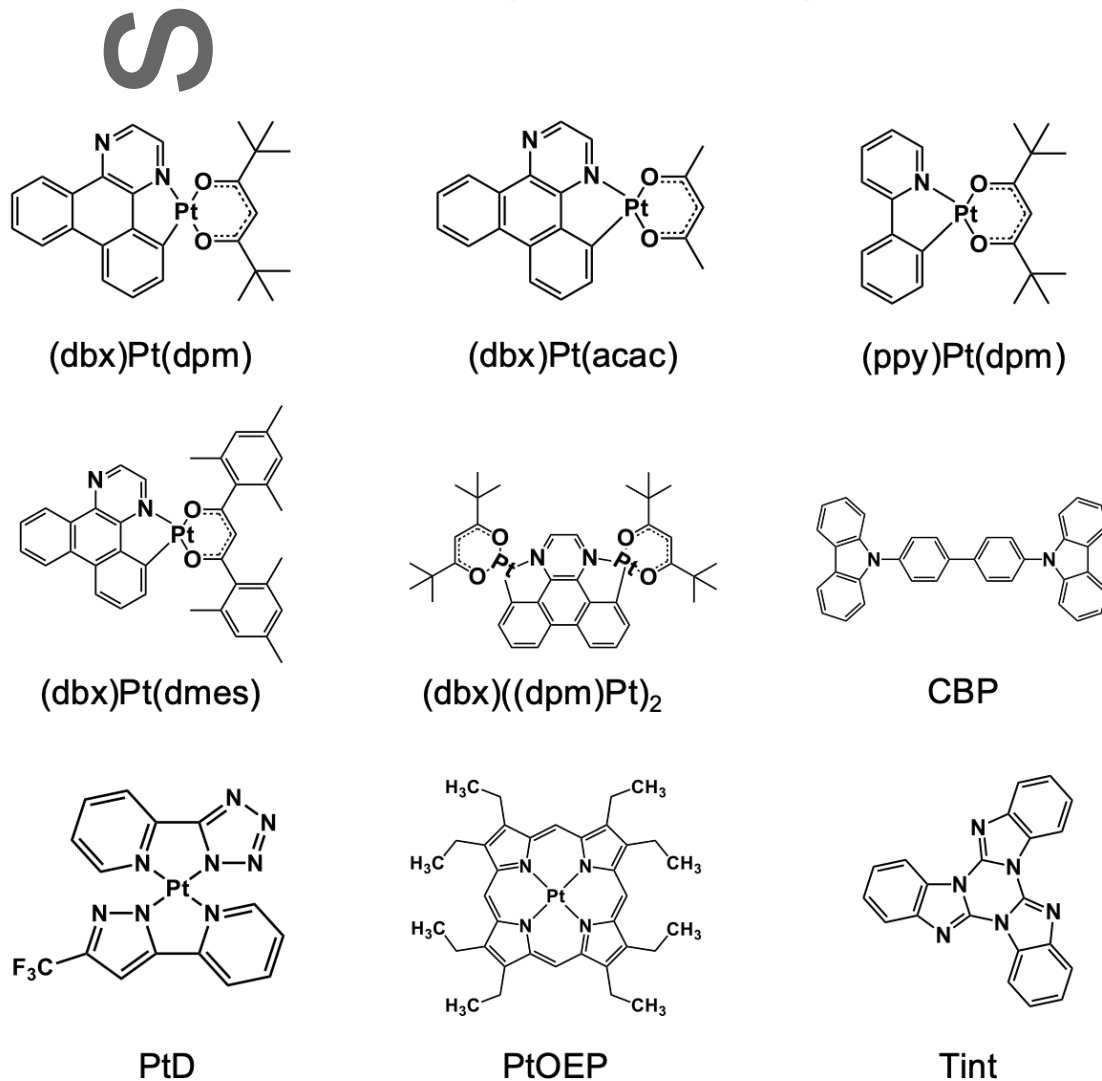


Figure 2

A

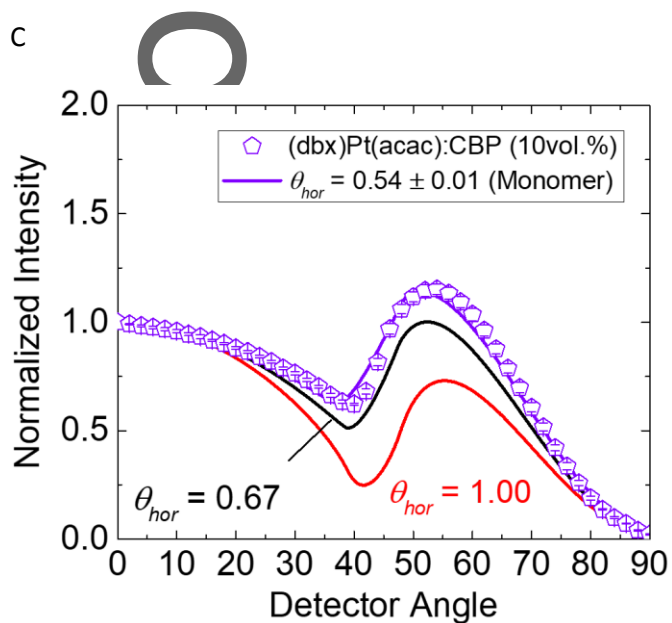
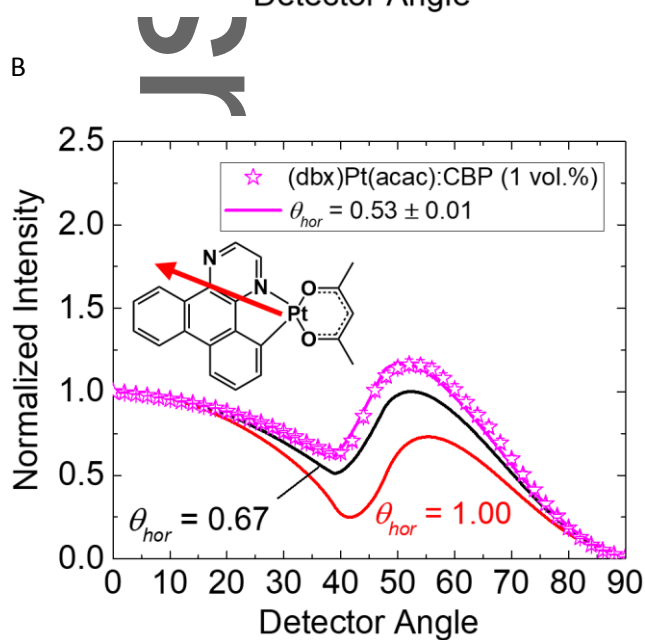
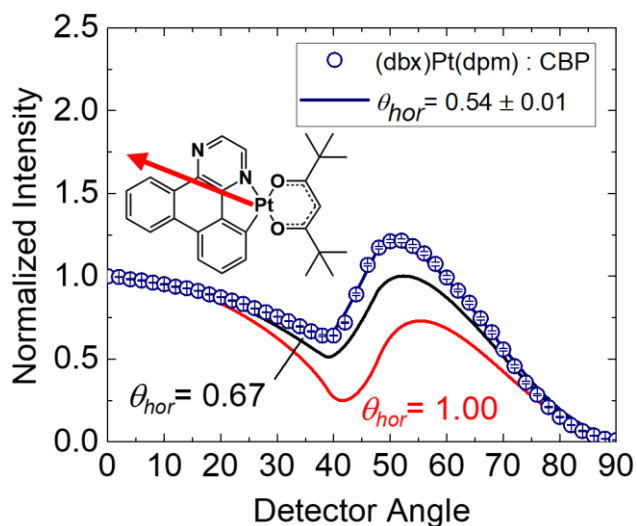
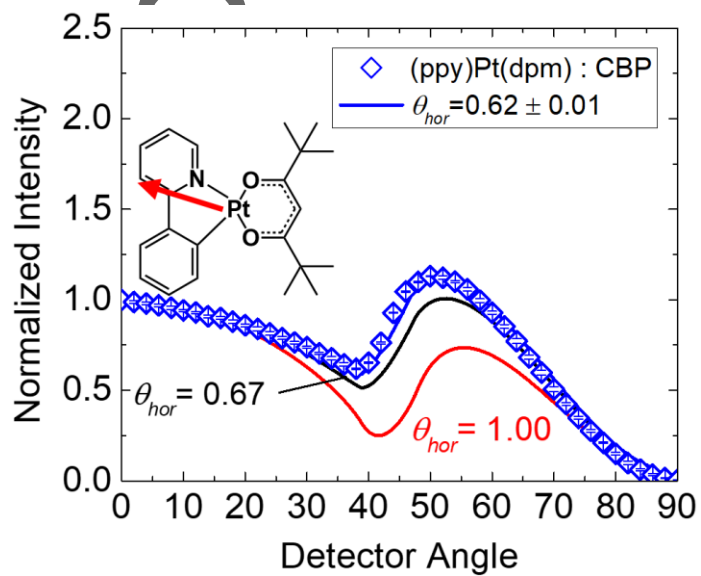
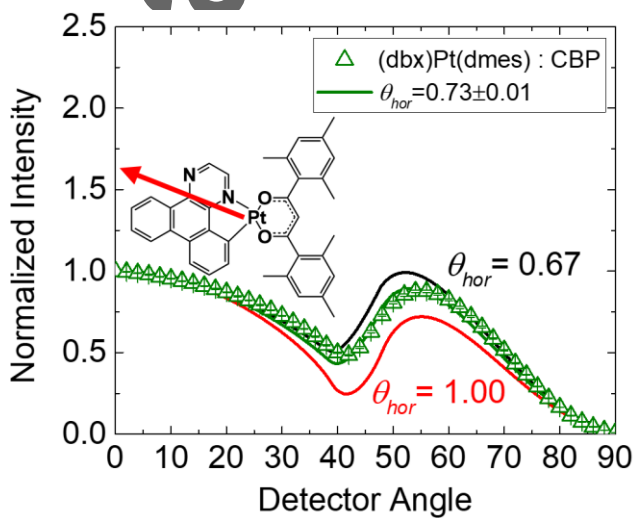


Figure 3

A



B



C

Aut

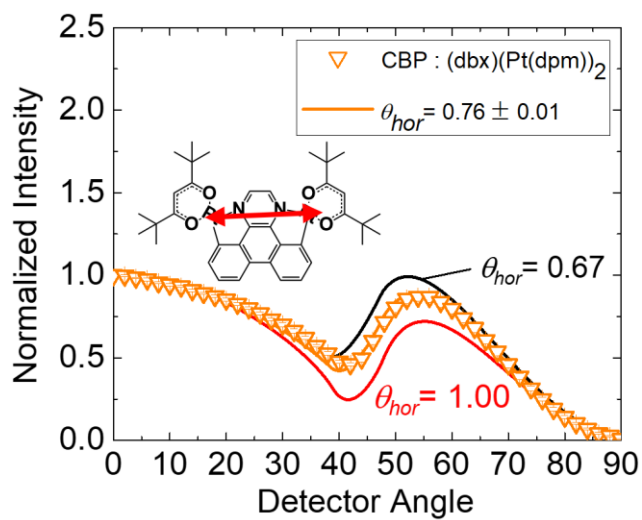


Figure 4

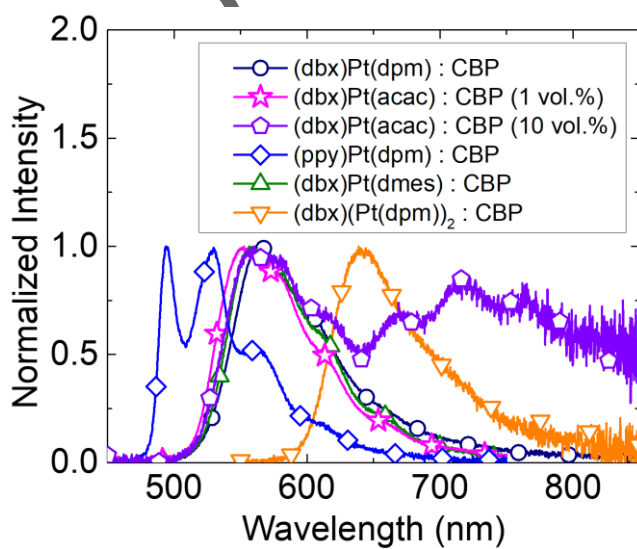


Figure 5

A

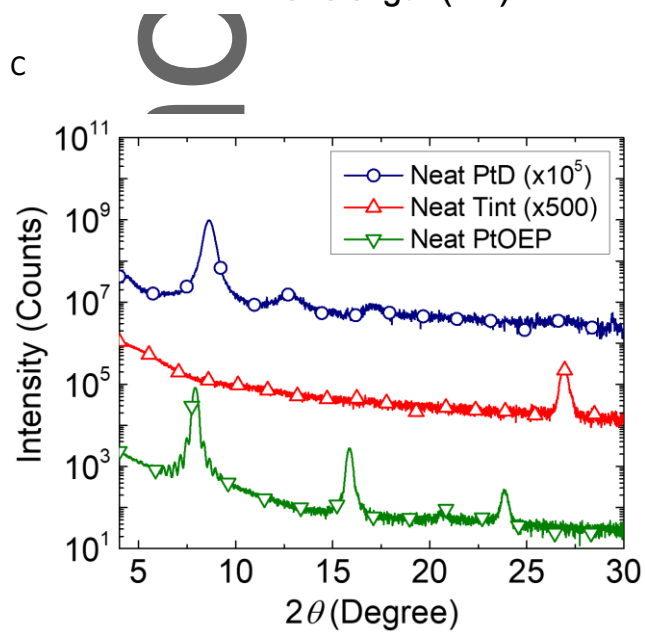
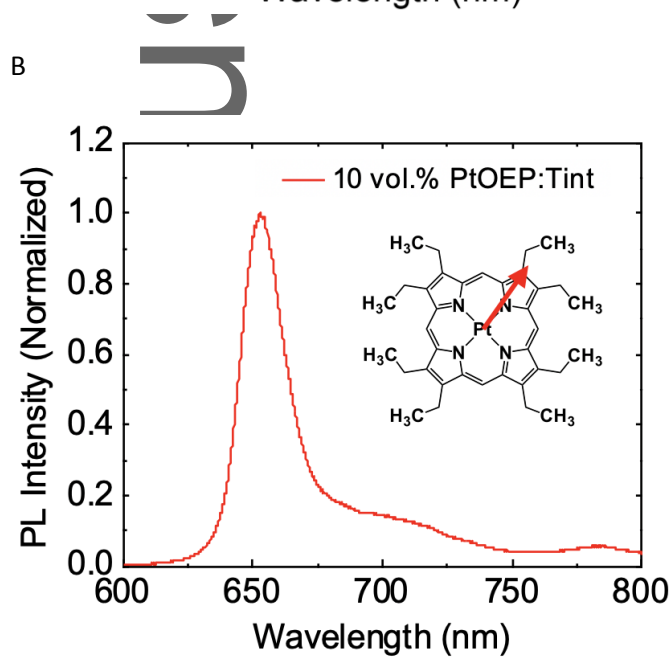
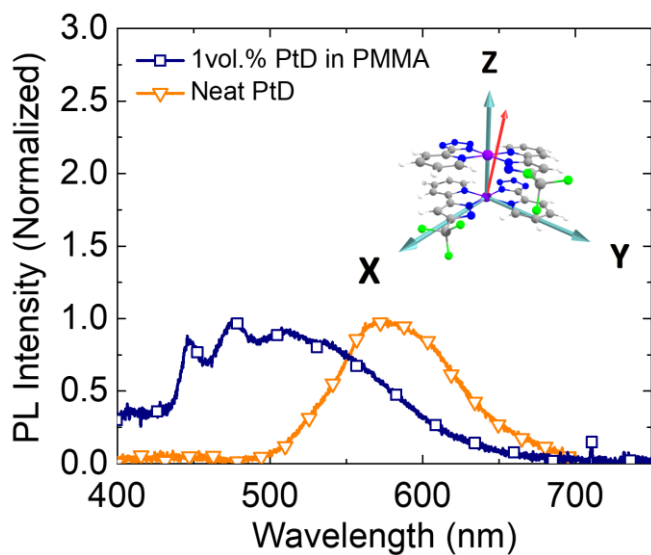
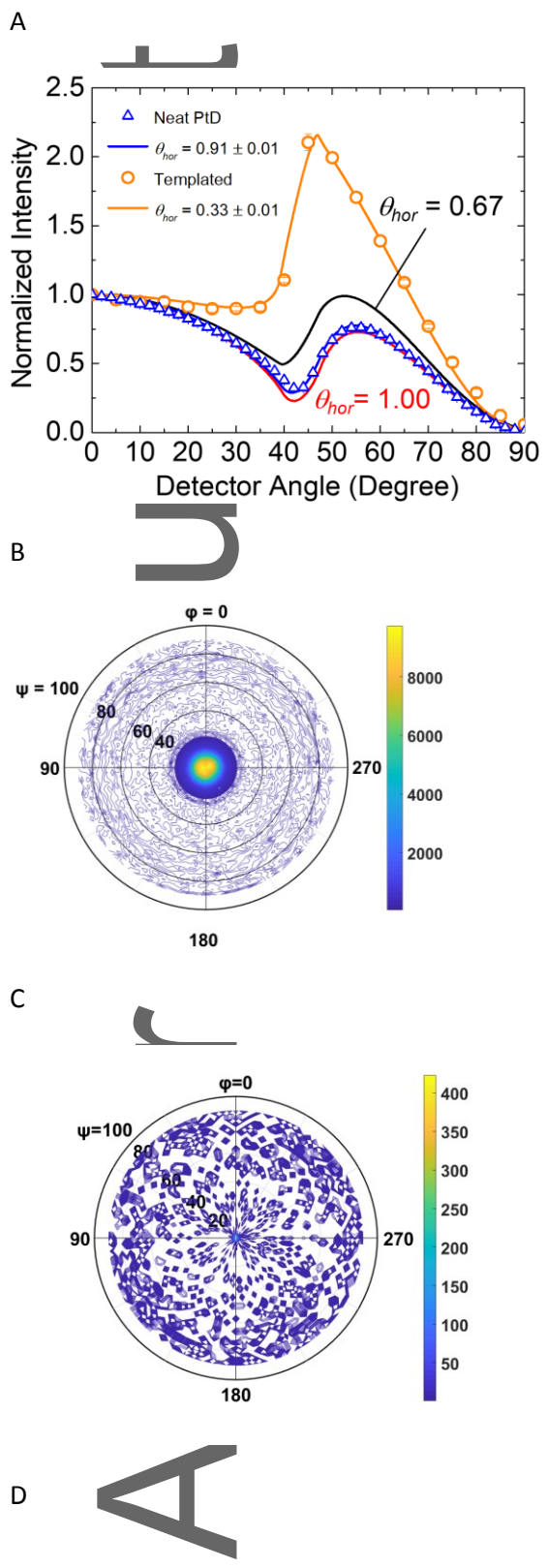


Figure 6



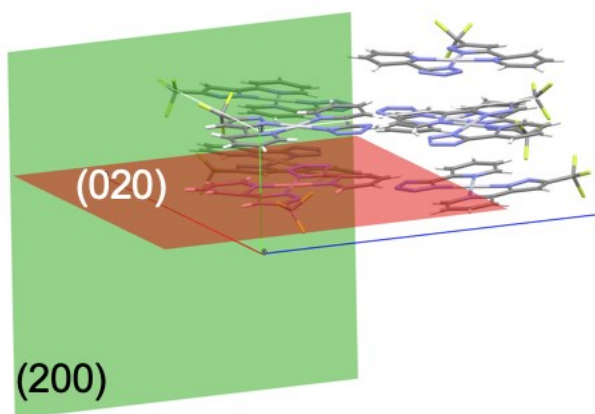
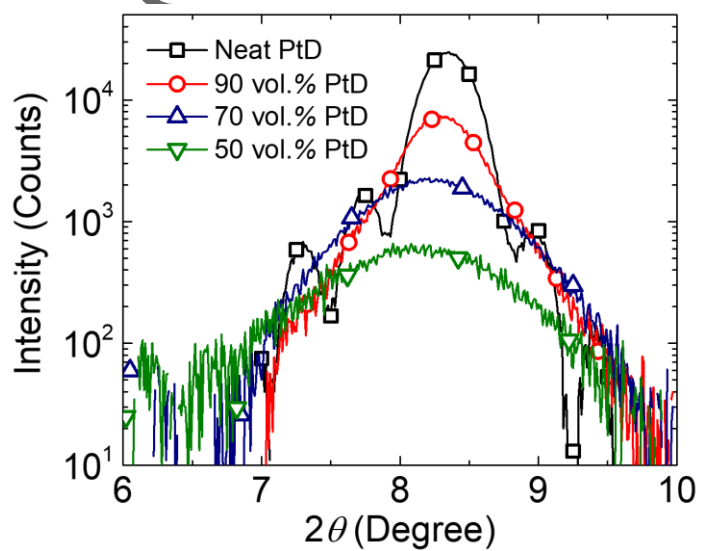


Figure 7

A



B

Auth

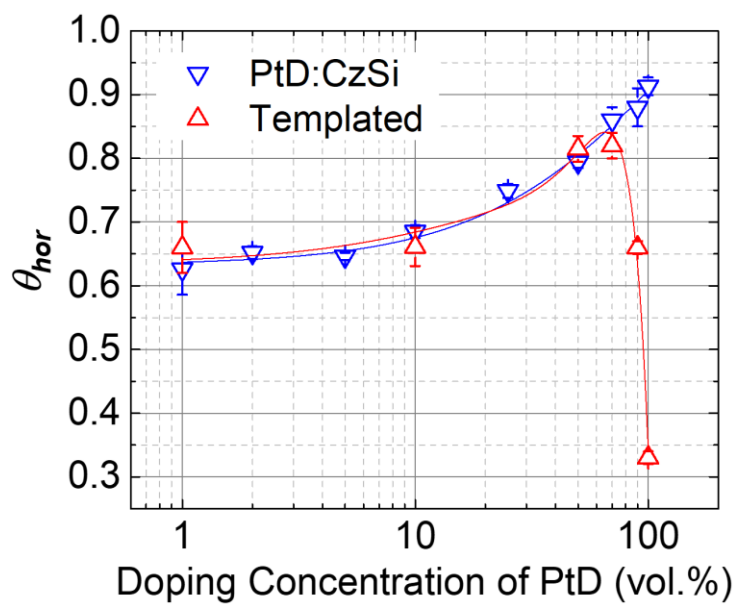
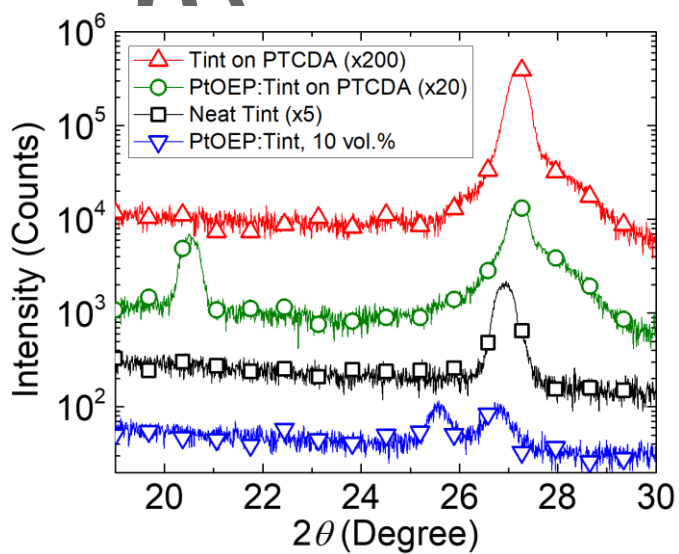


Figure 8

A



B

